Journal of Hazardous Materials Advances 21 (2026) 101093

Contents lists available at ScienceDirect

Journal of Hazardous Materials Advances

journal homepage: www.elsevier.com/locate/hazadv

The effect of crystallization kinetics on the fluorescence behavior of label-free PET nanoplastics: ecotoxicological relevance for freshwater zooplankton

Francesca Lionetto [a,*], Gregorio Polo [b], Sonia Bagheri [a], Claudio Mele [a], Carola Esposito Corcione [a], Maria Giulia Lionetto [b]

[a] Department of Engineering for Innovation, University of Salento, Lecce, Italy
[b] Department of Biological and Environmental Sciences and Technologies (DiSTeBA), Lecce, Italy

ARTICLE INFO

Keywords:
Polyethylene terephthalate
Crystallization kinetics
Nanoplastics
Autofluorescence
Freshwater zooplankton
Climate warming
Thermal tolerance

ABSTRACT

Nanoplastics (NPs) are pervasive pollutants whose detection and collection from the environment is challenging due to their extremely small size, which limits the effectiveness of characterization techniques. This study analyses the impact of crystallization kinetics on the autofluorescence behavior of unlabeled polyethylene terephthalate (PET) NPs produced by mechanically fragmenting plastic waste in conditions that simulate natural degradation. This process yields particles with properties similar to those found in nature. By studying crystallization kinetics, it is possible to restore polymer crystallinity, effectively replicating the increased crystallinity observed in environmentally degraded polymers. Additionally, the enhanced crystallinity leads to a stronger fluorescence signal allowing the resulting nanoparticles to be used without additional fluorescent staining, a novel feature that overcomes the limitations of conventional dye labelling.

The ecotoxicological relevance of the obtained label-free PET nanoplastics is validated through in vivo exposure on the freshwater zooplanctonic model species *Daphnia magna* at two different temperatures. Confocal microscopy indicates a prevalent accumulation in the gastrointestinal tract. Recovery results reveal a clear decline in organism survival that is dependent on both dose and temperature, indicating that higher temperatures amplify the toxic effects of PET nanoparticles. This highlights the potential for global warming to exacerbate the ecological impacts of microplastics.

1. Introduction

Micro and nanoplastics (MNPs) are pervasive pollutants found in different environments, including urban areas, remote regions, aquatic ecosystems and indoor dust (Yang et al., 2023). Their concentrations vary significantly ranging from 10^3 items·m^{-3} to 10^4 items·m^{-3}, in different surface water environments (Eo et al., 2019; Cheng et al., 2021). Aquatic environments are particularly at risk for MNPs contamination due to the widespread use and poor disposal of plastics, which break down into smaller particles that persist in water bodies (Besseling et al., 2019; Chae and An, 2017). These tiny plastics are now found globally in both marine and freshwater systems, where they can be ingested by a wide range of aquatic organisms, from algae and invertebrates to fish. Their small size allows them to be easily taken up by organisms and transferred through food webs (ref) with potential risks for human health. Micro- and nanoplastics are highly motile in the environment and can also adsorb and transport other environmental contaminants, increasing the risk of toxic exposure for aquatic life and potentially altering the toxicity and bioavailability of these chemicals (Serra et al., 2025; Patrício Silva et al., 2024). The pervasive distribution of MNPs raises serious concerns about their impact on ecosystems and human health. Particularly, nanoplastics, typically defined as plastic particles ranging from 1 to 1000 nanometers (Gigault et al., 2018) raise significant concerns due to their small size, which allows them to interact with biological macromolecules (Polo et al., 2024), cross cell membranes (Giordano et al., 2025; Hua and Wang, 2022), penetrate biological barriers (Bai et al., 2024), and accumulate in tissues and organs (Nihart et al., 2025; Dong et al., 2023), representing potential treat for the health of wildlife and humans (Chang et al., 2020). Aquatic species are especially vulnerable, and current evidence suggests that the

* Corresponding author.
E-mail address: francesca.lionetto@unisalento.it (F. Lionetto).

https://doi.org/10.1016/j.hazadv.2026.101093
Received 31 July 2025; Received in revised form 13 November 2025; Accepted 21 January 2026
Available online 19 February 2026

concentrations of MNPs in some areas may already pose ecological risks (Besseling et al., 2019). The persistence and ubiquity of micro- and nanoplastics, combined with the potential risks for humans and wildlife highlight the urgent need for improved monitoring, assessing their impact, and mitigation strategies

Micro- and nanoplastic sampling faces challenges like limited site access, inconsistent methods, small sample volumes, and contamination risks (Nakano et al., 2025). The lack of standard protocols and environmental variability hinder data comparability and representativeness. Their extremely small dimensions limit the effectiveness of standard characterization techniques. In environmental samples, NPs are often mixed with various polymers and additives, making accurate identification and analysis even more difficult. Furthermore, NPs are often found in complex environmental matrices, such as sediments, water, and biological tissues, that can interfere with detection methods. Current analytical methods are not sufficiently adapted or validated for these contexts, resulting in a lack of reliable techniques for NP identification and quantification. Additionally, NPs tend to aggregate and may undergo chemical transformations over time, further complicating systematic studies of their properties and effects (Lettieri et al., 2025).

Simplified model NPs, mostly polystyrene (PS) NPs, are commonly used in environmental impact studies. However, their relevance is limited because they differ significantly from real-world NPs in both physicochemical properties and shape. Unlike naturally occurring NPs, model NPs are typically monodisperse, spherical and chemically functionalized, and do not accurately represent the diversity of polymers, shapes, and surface chemistries found in nature (Ramsperger et al., 2022). Additionally, toxicity effects may often be driven more by the surfactants used than by the particles themselves (Ramsperger et al., 2022). The World Health Organization (WHO) has emphasized the need for test MNPs materials with greater environmental relevance, encompassing a diversity of polymer types, morphologies, and physicochemical properties (World Health Organization 2022). A major limitation in many toxicity studies is the insufficient characterization of test materials, which undermines their utility for risk assessment (Santizo et al., 2025). These challenges underscore the need for NPs with well-defined, reproducible, and environmentally realistic properties to better simulate exposure scenarios and support meaningful ecotoxicological assessments.

Understanding the behavior and impacts of nanoplastics requires the use of reproducible model nanoplastics for controlled laboratory studies. Two main approaches are employed to produce these materials: top-down and bottom-up methods. Top-down techniques, such as milling, ultrasonication, and laser ablation, fragment bulk plastics into smaller particles while preserving their chemical composition (Ducoli et al., 2025), whereas bottom-up approaches, including emulsion polymerization, solvent evaporation, and nanoprecipitation, synthesize nanoplastics from monomers or dissolved polymers, yielding uniform and size-controlled particles (Crosset-Perrotin et al., 2025). Among top-down methods, milling stands out as a versatile mechanical technique capable of reducing macroplastics to nanoscale fragments while maintaining their chemical integrity (Lionetto et al., 2022; Ducoli et al., 2024; Rajabimashhadi et al., 2024). Although milling often requires cryogenic pretreatment and long processing times, and may yield limited quantities of particles smaller than 100 nm, it represents an effective approach for producing environmentally relevant and irregularly shaped particles. Overall, ball milling stands out as a key method for generating realistic model nanoplastics by mechanical reproducing the combination of forces that mimic the natural plastic fragmentation driven by wave erosion and rock impact (Giordano et al., 2025; Ducoli et al., 2024).Many polymers that form MNPs are semicrystalline, making the study of microplastic crystallinity essential, as it significantly influences their physical properties and degradation behavior. The degree of crystallinity in MNPs can vary based on the type of polymer and the conditions under which it was degraded. In natural environments, weathering often leads to an increase in crystallinity because the amorphous regions degrade faster, exposure to UV light accelerates chain scission, breaking polymer chains into smaller fragments with a higher mobility allowing them to reorganize into crystalline regions (Aljoumaa and Abboudi, 2015). Despite its importance, to the authors knowledge, research on microplastic crystallinity still remains very scarce. Understanding this aspect is critical, as crystallinity affects not only degradation rates but also can influence their interactions with living organisms. Typically, higher crystallinity results in greater resistance to environmental degradation, allowing microplastics to persist longer in the environment. Therefore, studying microplastic crystallinity is vital for understanding MNPs environmental behavior, their interaction with living organism and developing strategies to mitigate plastic pollution in aquatic environments.

Among MPs, polyethylene terephthalate (PET) is one of the most prevalent and environmentally persistent types. PET is one of the most widespread polymer with a global production reaching 28 million tons in 2024 (Jovanović et al., 2025) covering a broad range of applications, from bottles, food containers, and packaging to textile fibers and advanced industrial composites (Greco et al., 2015). Despite recycling efforts, less than half of PET waste is recovered, leading to environmental accumulation through both degraded products (secondary MPs) and direct sources like fibers and glitters (primary MPs) (Alaraby et al., 2025; Briga-Sá et al., 2023). PET microplastics (MPs) are prevalent in soils, sediments, dust, and water, even reaching remote areas (Kumar et al., 2024). For examples, PET has been identified as the most prevalent polymer MPNPs in East Greenland fjords (Vetter et al., 2025). PET MNPs contaminate drinking water and seafood, and bioaccumulate across food chains (Rajtar et al., 2025). NPs are easily transported in the environment, can sorb and release pollutants, (Lionetto et al., 2022). Aquatic organisms suffer ingestion, toxicity, reproductive harm, and behavioral changes due to MPs, ultimately disrupting ecosystems.

PET MNPs can absorb a variety of pollutants from the surrounding environment due to their large surface area and hydrophobic nature. In long-term studies, PET showed a significant increase in PFAS adsorption, suggesting a possible diffusion process of PFAS within the polymer matrix (Freilinger et al., 2025). Aged PET MPs have been reported to absorb more pharmaceutical contaminants than unaged ones, primarily due to hydrogen bond formation as recently demonstrated between amoxicillin and ester groups of PET microplastics (Lionetto et al., 2023). Humans are exposed through ingestion and inhalation, and recent studies have detected various MPs in human feces (Yang et al., 2023) and placenta (Liu et al., 2023), with PET being among the most common. PET degrades slowly, causing long-term accumulation in ecosystems and increased human exposure risk; environmental factors like pH can further increase toxic chemical leaching (Giordano et al., 2025). Given its widespread use, the potential health risks of PET MNPs merit close attention.

MNPs in biological samples are typically visualized by fluorescence imaging usually after staining with fluorescent dyes. However, these dyes can introduce limitations such as non-specific signals, false positives, photobleaching, and dye leaching (Cho et al., 2025). Recent works have shown that PET nanoparticles exhibit intrinsic autofluorescence, enabling their detection without the use of external dyes and preserving their native properties (Lionetto et al., 2022). The intrinsic fluorescence of PET nanoparticles offers promising potential for tracking nanoplastics in environmental samples and studying their cellular interactions, without the complications introduced by external labeling (Giordano et al., 2025). This label-free imaging approach relies on the natural fluorescence arising from aromatic rings in the PET molecular structure, although further investigation is still needed to fully understand and enhance this phenomenon.

This study primarily aims to investigate the impact of crystallization kinetics on the autofluorescence behavior of PET micro- and nanoplastics (MNPs) produced by mechanically fragmenting plastic waste in conditions that simulate natural fragmentation forces like wave erosion and rock impact. This represents a novel and underexplored approach in

microplastic research that provides new insights into how structural transitions influence optical properties in environmentally relevant plastic particles. The study examines how thermal treatments influence crystallinity and explores the effect of crystallinity levels on autofluorescence intensity through the application of multiple analytical techniques. Another goal is to restore polymer crystallinity by mimicking the increased crystallinity of degraded polymer in the environment. Finally, the suitability of label-free PET nanoplastics for biological studies and their impact on aquatic organisms has been assessed using in vivo exposure experiments on neonates of the freshwater zooplanctonic model species *Daphnia magna* and ecotoxicological outcomes have been investigated under different exposure temperatures.

Daphnia magna, a species of freshwater zooplankton, represents a model organism due to its well-known biology, short lifecycle, parthenogenetic reproduction, and high sensitivity to pollutants (Ebert, 2022). The transparency of its body allows for easy physiological observation (Ducoli et al., 2025). As a primary consumer and prey for higher trophic levels, *Daphnia magna* plays a vital role in aquatic food webs. As a filter feeder, Daphnia naturally ingests MNPs present in the water column (Le et al., 2016), reflecting realistic exposure scenarios. *Daphnia magna* serves as a bioindicator for assessing the impact of various environmental stressors, including emerging contaminants such as nanoplastics, on aquatic ecosystems (Crosset-Perrotin et al., 2025) supporting its use in environmental risk assessment (Rosner et al., 2024).

2. Experimental

2.1. Nanoplastic production

Post-consumer PET bottles were used to prepare PET nanoparticles in this study. A sketch of the process is reported in Fig. 1. After cutting the bottles into pieces of about 5 × 10 cm^2, they were crushed in a Retsch SM 2000 cutting mill (RETSCH GmbH & Co., Düsseldorf, Germany). The obtained millimetric powder was finely milled to the micrometric size using a RETSCH ZM100 Ultra Centrifugal mill (RETSCH GmbH & Co., Düsseldorf, Germany) at 14.000 rpm. The micrometric powder was wet-milled at 390 rpm for 30 min in a zirconia jar, using ultrapure water and zirconia balls in an ambient atmosphere and an S/1 1000B ball mill (Ceramic Instruments S.r.l, Sassuolo Modena, Italy) with parameters optimized in a previous work (Lionetto et al., 2021). From previous studies (Rajtar et al., 2025), we found that approximately 60 % of the overall particle volume exhibited sizes within the nanometric range after 20 min of milling, whereas the micron-sized fraction resulted from incomplete comminution or particle aggregation. The suspension was subsequently sieved to remove particles larger than 1 μm and sonicated to ensure a homogeneous nanoplastic dispersion.

2.2. Atomic force microscopy (AFM)

Atomic force microscopy (AFM) was used to analyse the topography of PET nanoplastics. The characterization was performed with a Bruker MultiMode 8 AFM system. Ultrapure water was used to dilute the colloidal suspension of nanoparticles and 50 μL of the dispersion was spin-coated onto a steel disc, followed by drying at room temperature. AFM imaging was conducted in PeakForce QNM mode, under ambient conditions, utilizing RTESPA-300 cantilever (Bruker) with a spring constant of 40 N/m. In this mode, the AFM tip periodically tapped the surface and the tip-sample interaction force was directly controlled and measured in each tap. This mode was particularly useful in studying polymer samples because it combined mechanical mapping with minimal sample disturbance (Chang et al., 2023). The scan sizes were 3 × 3 μm^2 and 2 × 2 μm^2, the scan rate was 0.46 Hz and the resolution was 500 lines per scan. Data processing and size measurements were performed using Nanoscope Analysis v1.5 software (Bruker). The statistical analysis of nanoplastic sizes was performed by measuring the particle diameters and area by using ImageJ software on >500 nanoparticles.

2.3. Laser diffraction

Particle size distribution was analyzed using a CILAS 1190 multilaser particle size analyzer (CPS Us, Inc., Madison, WI, USA) in combination with Particle Expert® software. Powder samples were dispersed in a 500 mL water cell and illuminated by a low-intensity laser beam. The scattered light was collected and focused onto detectors using a Fourier lens, and particle size measurements were calculated based on Mie scattering theory. The results were the average of three replicates.

2.4. Differential scanning calorimetry

Thermal analysis was carried out using a METTLER TOLEDO DSC 822e under an inert nitrogen atmosphere with a flux of 60 ml/min. The instrument was calibrated with indium and aluminum pans of 40 μl were used. The analyzed samples consisted of two types: disks (6 mm in diameter) punched from post-consumer PET bottles (named PET-B) and

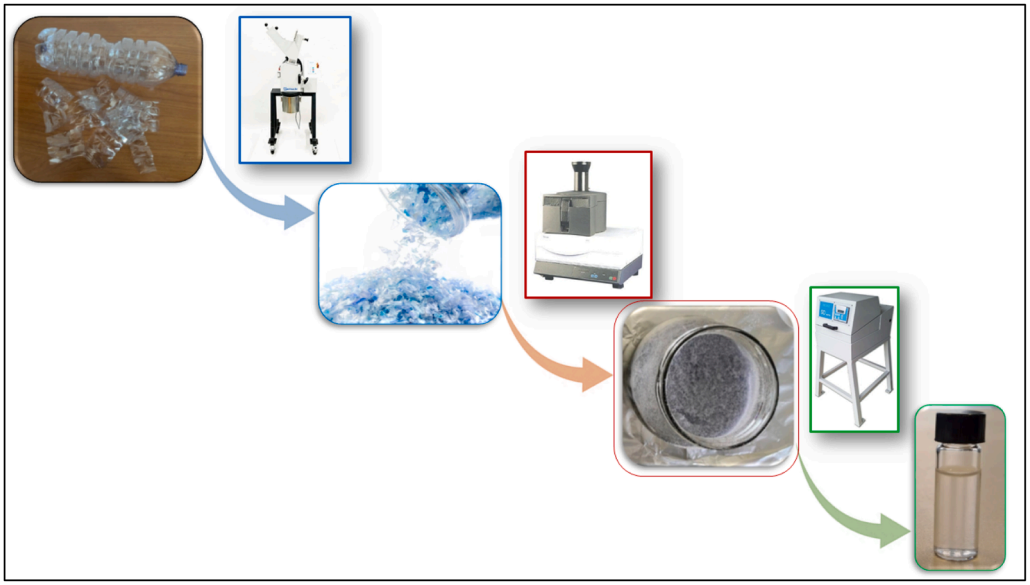

Fig. 1. Scheme of nanoplastic production process.

microplastic-like powder (designated as PET-MP) with an average particle size of 100 μm. Dry PET microparticles were used for DSC analysis instead of nanoparticles due to the experimental challenges associated with accurately handling and weighing nanoparticle samples, while microparticles provide sufficient mass and reliable thermal signals representative of the polymer's bulk behavior. As reported in the literature, DSC allows reliable identification and quantification of semicrystalline PET microplastics, with particle size affecting peak resolution but not the intrinsic thermal transition temperatures which are independent of sample morphology or size scale (Rodríguez Chialanza et al., 2018; Šudomová et al., 2023). Samples of about 7–10 mg were heated from 25 °C to 300 °C at 10 °C/min followed by cooling from to 25 °C and second heating, both at 10 °C/min. A Sartorious balance with a weighing accuracy of 0.01 mg was used. The glass transition temperature, T_g, of each sample was defined as the inflection point of the glass transition heat flow jump. The melting temperature was defined as the peak temperature of the melting endotherm. The annealing procedure was studied by applying the following protocol: heating from 60 °C to annealing temperature at 10 °C/min, holding 2 h at annealing temperature, cooling to 25 °C at 10 °C/min and subsequent heating from 25 °C to 280 °C at 10 °C/min. The annealing temperature was varied between 100 °C and 160 °C. Each result was the average of three replicates.

2.5. Raman spectroscopy

Raman spectroscopy was carried out using a LabRam confocal system (Horiba Jobin Yvon) equipped with a 100 × objective lens. A He–Ne laser working at 633 nm supplied 7 mW at the sample surface. Spectral acquisition was performed with a 3 cm^{-1} spectral resolution over a wavenumber range of 100–2000 cm^{-1} with 300 scans per sample.

2.6. Spectrofluorimetric analysis and confocal fluorescence microscopy visualization of PET NPs

The fluorescence emission spectra of aqueous dispersions of label-free PET nanoparticles were measured with a Cytation 5 multimode reader (BioTek, Winooski, VT, USA) in Corning® 96-Well Black Microplates (Glendale, AR, USA) in the λ range from 350 nm to 700 nm.

The fluorescence microscopic visualization of PET NPs powder aggregates was performed by using confocal analysis. Briefly, 0.2 mg of PET NPs powder was spread on the surface of a microscope slide, mounted with IBIDI mounting medium for fluorescence microscopy (Ibidi GmbH, Gräfelfing, Germany) and visualized by 405 nm laser lines of A1 NIKON (Tokyo, Japan) confocal laser scanning unit coupled with a NIKON Ti microscope using a Plan Apo 60 × 1.40 Oil objective (Nikon, Tokyo, Japan).

2.7. Short term exposure of Daphnia magna to PET NPs and recovery

The ecotoxicological impact of PET NPs on the model organism *Daphnia magna* were evaluated by exposing hatched neonates <24 h old to PET NPs in the concentration range from 5 mg/L to 100 mg/L for 48 h and recording mortality as endpoint according to EN ISO 6341:2012 (EN ISO 6341 2012). The choice of neonates is guided by standard ecotoxicological protocols (e.g., OECD Test Guideline 202 (Development, O. for E.C 2004)) and optimizes the sensitivity, reproducibility, and ecological relevance of the tests. Neonates represent the early stage of life, which is the most vulnerable phase of an organism's life cycle. Impacts on neonate survival and development directly affect population sustainability, making them ecologically relevant endpoints (David et al., 2011).

Daphnids were derived from Daphtoxkit F™ magna (1996) conform with ISO Standard 6341and OECD Guideline 202 (Development, O. for E.C 2004). The organisms were prefeed with lyophilized *Arthrospira platensis* provided by the kit. Two exposure experiments were performed in parallel at two different temperatures: one at 21 ± 1 °C and the other at 25 ± 1 °C under a 16: 8 h light/dark regime. Control organisms were exposed to the same experimental conditions as test organisms except for the presence of PET NPs. ASTM synthetic water was used for experiments (ASTM, 1980). 21 ± 1 °C is included in the normal culture temperature for these organisms, since their optimal temperature range is typically between 18 and 22 °C, according to OECD Guideline 202 (Development, O. for E.C 2004). 25 ± 1 °C is often used in experiments with *Daphnia magna* to simulate an increase in environmental temperature since 25 °C represents a moderate thermal stress condition, mimicking the effects of climate change or heatwaves in freshwater ecosystems (Bergman Filho et al., 2011; Im et al., 2020). Before exposure of *Daphnia*, the dispersion of PET NPs in ASTM water was sonicated with a customized protocol using a Bioruptor Plus (Diagenode, Denville, NJ, USA) to improve the nanoparticle dispersion. After 48 h of exposure, daphnids were inspected for immobility (according to EN ISO 6341:2012 (EN ISO 6341 2012)) and immobilized organisms counted. Immobilization was assumed when the animals cannot swim within 15 s when gently prodded (Development, O. for E.C 2004). Mortality was expressed as the percentage of immobilized animals for each concentration and each temperature condition.

After 48 h exposure, live organisms were first transferred to clean ASTM water to rinse them and subsequently transferred to clean ASTM water with added algae (*Clorella vulgaris*; density 5 × 10^4 cells) for another 48 h under the same conditions as during the first 48 h (at two temperatures 21 °C and 26 °C under a 16: 8 h light/dark regime). After 48 h of exposure, mortality was recorded.

2.8. Visualization of PET NP in the body of Daphnia magna

The visualization of PET NP in the body of *Daphnia magna* neonates was performed after 24 h exposure to PET NPs 5 mg/L. After the exposure, the organisms were first transferred to clean ASTM water to rinse them before visualization. Then they were put in a small drop of ASTM water into the wells of a Corning 96 multiwell black. Images of the whole organisms were taken at 4 × magnification under bright field and fluorescence microscopy observation using a Cytation 5 (BioTeck Winooski, VT, USA) imaging multi-mode reader provided with 360/460 nm (blue) filter set. The visualization was performed in 5 replicates

3. Results

3.1. Morphological characterization and size distribution of PET nanoparticles

The procedure employed in this study enabled the production of nanoparticles without the use of toxic solvents, while also simulating the fragmentation of plastic debris in aquatic environments caused by mechanical abrasion. The morphology of the resulting nanoparticles is shown in Fig. 2a-b). These nanoplastics were irregularly shaped, similar to naturally occurring nanoplastics. They were not perfectly spherical but rather elongated. Circularity analysis was performed using ImageJ software on several AFM images. The software calculated circularity according to the following equation:

$$Circularity = \frac{4 * \pi * Area}{(Perimeter)^2} \quad (1)$$

with a circularity value of 1 indicating a perfect circle. The shape observable in Fig. 2a-b are consistent with an obtained circularity value of 0.68 ± 0.11.

The size distribution of PET particles generated during the milling process was analyzed using both AFM and laser diffraction techniques, showing a right-skewed distribution centered around 150–200 nm, with most particles below 400 nm. The frequency distributions shown in Figs. 2c–d represent the probability of encountering a particle with a given diameter (D) within the sample population. Key percentile values

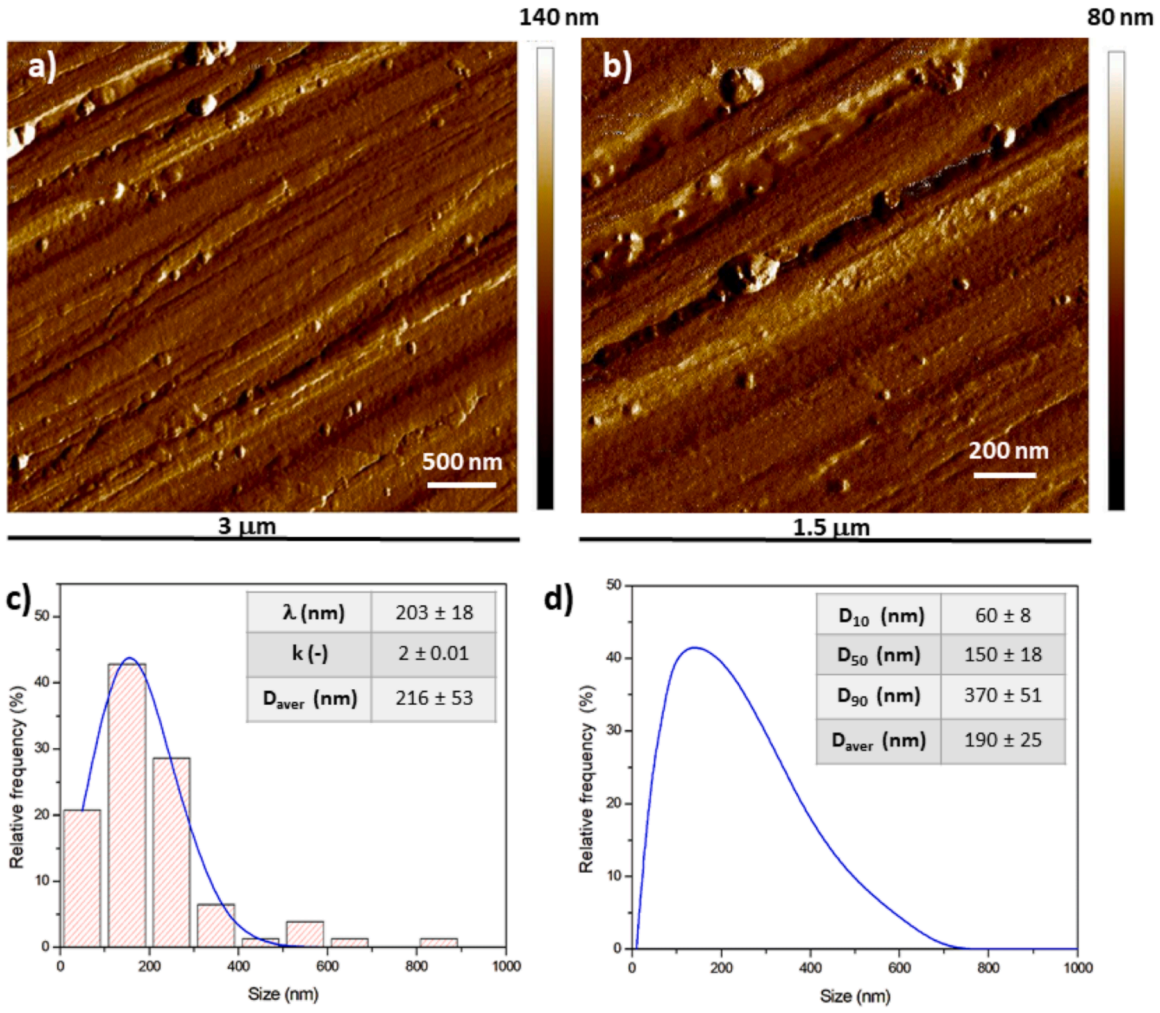

Fig. 2. a, b) AFM images of PET nanoparticles at two different magnifications; c) particle size distribution obtained from AFM image analysis; d) particle size distribution measured by laser diffraction.

(D_{10}, D_{50}, and D_{90} in Fig. 2d) indicate the diameters below which 10 %, 50 %, and 90 % of the total particle volume are found, respectively. The consistency between AFM and laser diffraction confirms the reliability of the size estimation across methods.

Moreover, particle size distribution resulting from AFM measurements, was modeled with Weibull distribution (De Pascalis et al., 2023):

$$f(l) = \frac{k}{\lambda}\left(\frac{l}{\lambda}\right)^{k-1} \exp\left[-\left(\frac{l}{\lambda}\right)^{k}\right] \quad (2)$$

where k an λ were the shape and scale parameter, respectively. These parameters were obtained by applying the least square method to the

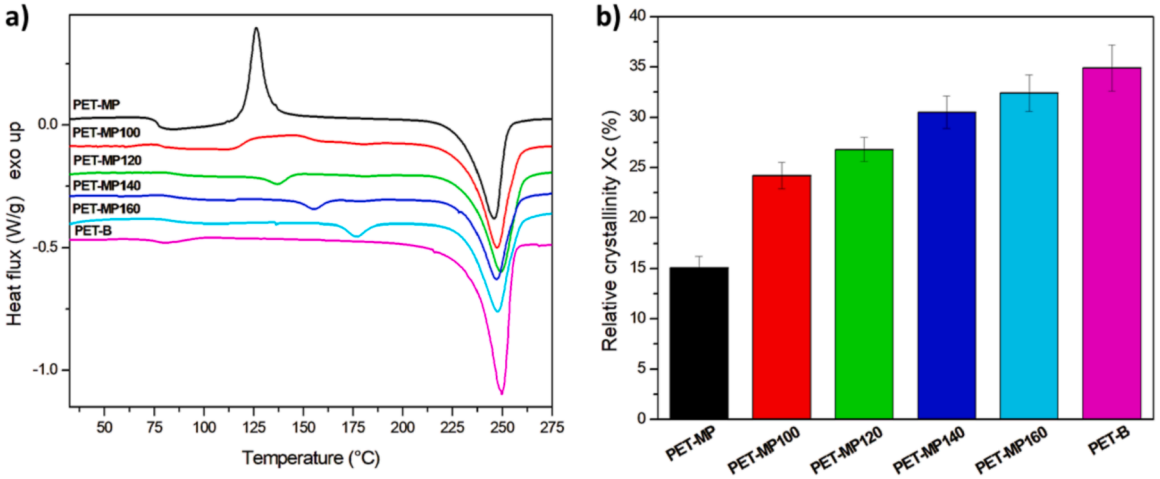

Fig. 3. a) DSC thermograms of PET microplastics and post-consumer bottle, before and after 2 h annealing at different temperatures; b) apparent crystallinity.

size measurements from AFM images and are reported in Fig. 2c. The fitted length parameter, λ, closely matched the average particle size determined by laser diffraction.

The shape parameter ($k = 2$) indicated a moderately skewed distribution with a distinct peak centered around a dominant particle size. Such a distribution is characteristic of breakage processes governed by brittle fracture mechanics, where particle fragmentation occurs in a relatively uniform manner.

3.2. Isothermal crystallization kinetics of PET microplastics

Fig. 3 compares the thermal behavior of PET microparticles, analyzed by DSC at a heating rate of 10 °C/min, with that of the original post-consumer PET bottles. The glass transition temperature (T_g) was identified as the inflection point on the DSC curve, corresponding to the change in heat capacity. For the PET bottle samples (labeled PET-B in Fig. 3a), the glass transition occurred at 77 °C, and the melting endotherm peak was at 249 °C.

DSC provide indirect indications on the formation of lower molecular weight species during PET milling by analyzing changes in the thermal properties of the material. Šudomová et al. (Šudomová et al., 2023) observed significant differences (about 20 °C) in peak temperatures of recycled PET samples under various conditions that may indicate alterations in molecular structure, including the formation of lower molecular weight species. However, in the thermograms reported in Fig. 3a, there is no significant difference in the melting peak temperature, as also reported in Table 1, confirming that the milling process did not produce a significant amount of lower molecular weight species.

Moreover, thermogravimetric (TGA) analysis in nitrogen at 10 °C/min revealed that both the PET bottle and the corresponding MPs exhibit a two-step decomposition process. The TGA curve of MPs closely resembles that of the PET bottle, although it is slightly shifted toward lower temperatures. This minor shift is likely due to PET degradation induced by mechanical fragmentation, as also reported by Ducoli et al. (Ducoli et al., 2024). In conclusion, within the limits of the sensitivity of DSC and TGA analyses, the milling process did not produce a significant amount of lower molecular weight species.The microparticles produced by milling (black curve, labeled PET-MP in Fig. 3a) exhibited an additional exothermic peak at 131 °C, corresponding to the cold crystallization of the amorphous regions of the molecular chains (Cheng et al., 2021). This indicated that the mechanical energy from milling induced amorphization in the PET polymer. The milling process applied significant mechanical stress, especially to the crystalline regions. Repeated impacts and shear forces disrupted the ordered arrangement of polymer chains, with the energy input eventually overcoming the forces that maintain the crystal structure. This transformation likely occurred in the solid state, as the temperature inside the milling jar rose above the polymer glass transition temperature but remained well below the melting point, consistent with observations from other studies (Font et al., 1999; Zaker and Auclair, 2024). As also reported by Bai et al. (Bai et al., 2000), the temperature during grinding allowed sufficient molecular mobility to promote solid-state amorphization without reaching the melt phase.

The heat absorbed during melting, ΔH_m, or released during crystallization, ΔH_{cc}, was proportional to the area between the curve and the baseline of the DSC thermogram in the temperature range where the transition occurred. The difference between ΔH_m and ΔH_{cc} corresponded to the heat associated with the melting of the crystals initially present in the sample. The relative crystallinity, X_c, was calculated according to Eq. (1):

$$X_c = \frac{\Delta H_m - \Delta H_{cc}}{\Delta H_0} * 100(\%) \quad (3)$$

were ΔH_m and ΔH_{cc} were the melting and cold crystallization enthalpies (J/g), respectively, and $\Delta H_0 = 140$ J/g the melting enthalpy of a 100 % crystalline PET (Lionetto et al., 2021; Viora et al., 2023; Androsch and Wunderlich, 2005).

The thermal properties are summarized in Table 1. The apparent crystallinity of PET-B (34.7 ± 2.2 %) was in agreement with literature data where a range of 25–38 % was observed for water bottles except for the finish/neck zone (Zaker and Auclair, 2024; Lu et al., 2022). The milled PET microplastics (PET-MP) presented a reduced crystallinity (15.1 ± 1.1 %).

Plastic waste and microplastics in the environment undergo weathering due to UV exposure and thermal ageing. In semi-crystalline polymers, the amorphous regions of the polymer chains degrade more readily than the crystalline regions, which are less accessible to environmental factors. As a result, the crystallinity of the remaining microplastic particles tends to increase over time (Thomsen et al., 2023; Guo and Wang, 2019). To accurately replicate environmentally relevant micro- and nanoplastics, it is essential to restore their original, pristine level of crystallinity. For this purpose, the crystallization kinetics of PET microplastics was studied by DSC and thermal annealing was applied in the temperature range of 100–160 °C, i.e. between T_g and T_m, to promote crystallization without melting the polymer but preserving its structural integrity. The samples were heated from 25 °C to the selected isothermal temperature at 60 °C/min, then they were kept for 2 h at the isothermal temperature, then cooled to 25 °C at 10 °C/min and heated to 280 °C at 10 °C/min. The labels used in Fig. 3 were PET-MP100, PET-MP120, PET-MP140 and PET-MP160 to indicate samples annealed at 100 °C, 120 °C, 140 °C, 160 °C.

The DSC thermograms in Fig. 3a revealed the effect of annealing treatment on the crystallization behaviour of PET microplastics. After isothermal annealing of microplastics at 100 °C (sample MP-100 in Fig. 3a), the crystallization peak was still present, even if its intensity was smaller than that of the milled samples. In samples annealed at temperatures above 100 °C, the exothermic peak disappeared but an additional small low-temperature endotherm was observed at approximately 15–17 °C above the annealing temperature in agreement with the literature (Bartolotta et al., 2003). This low-temperature melting indicated the occurrence of crystal perfection and reorganization during heating and the melting of less thermally stable crystallites likely formed during the isothermal treatment. The apparent crystallinity X_c was estimated accounting for the two observed melting enthalpies and the values plotted in Fig. 3b

The maximum of the main melting peak, observed at 247 °C for all annealed samples, remained unchanged in temperature regardless of annealing conditions while its enthalpy increased with the annealing temperature. As expected, the degree of crystallinity increased with the

Table 1
Thermal properties of PET microplastics and starting PET from post-consumer water bottles.

Sample	T_g (°C)	T_{lm} (°C)	T_m (°C)	ΔH_{lm} (J/g)	ΔH_m (J/g)	X_c (%)	RAF (%)
PET-B	77.2 ± 2.1	-	249.5 ± 1.1	-	48.6 ± 2.7	34.9 ± 2.3	56.3 ± 2.0
PET-MP	81.1 ± 0.6	-	247.6 ± 0.2	-	40.2 ± 1.9	15.1 ± 1.1	12.1 ± 1.3
PET-MP100	79.4 ± 0.4	-	247.5 ± 0.2	-	42.1 ± 1.8	24.2 ± 1.3	29.1±.4
PET-MP120	82.8 ± 0.6	137.1 ± 0.2	247.9 ± 0.3	2.4 ± 0.1	34.9 ± 1.6	26.8 ± 1.2	33.3 ± 2.1
PET-MP140	82.9 ± 0.6	155.5 ± 0.3	247.6 ± 0.4	2.7 ± 0.2	37.0 ± 2.1	30.5 ± 1.6	40.0 ± 2.9
PET-MP160	84.2 ± 0.9	174.8 ± 0.2	247.7 ± 0.3	3.8 ± 0.2	41.8 ± 1.8	32.4 ± 1.8	42.1 ± 3.9

annealing temperature since the existing crystalline regions grew further and additional crystallization occurred in the amorphous regions. This crystal perfection affected the T_g that increased from 79 °C to 84 °C.

To understand how crystallinity changes during annealing, the rigid amorphous fraction (RAF) was investigated. RAF represents the portion of the amorphous phase that is constrained by neighboring crystalline regions, exhibiting reduced mobility compared to a fully amorphous polymer. By analyzing the heat capacity change at the glass transition, the mobile amorphous phase MAF can be estimated according to this equation:

$$MAF = \frac{\Delta c_p}{\Delta c_p^0} \quad (4)$$

where Δc_p and Δc_p^0 were the specific heat capacity change of PET MPs and a 100 % amorphous PET at the glass transition, 0.405 J/(g K) (Badia et al., 2012), respectively. According to a three-fraction model, RAF was determined by the following equation (Corcione and Maffezzoli, 2009):

$$RAF = 100 - X_C - MAF \quad (5)$$

The RAF values at different annealing temperatures are reported in Table 1. A clear trend of increasing RAF with annealing temperatures indicates that more amorphous chains become immobilized at crystal interfaces and crystallization is dominated by formation of many small crystallites.

The evolution of relative crystallinity as a function of time at different annealing temperatures is presented in Fig. 4a. The data were modelled with the Avrami equation (Avrami, 1939):

$$X_c(t) = 1 - e^{-(kt)^n} \quad (6)$$

where $X_c(t)$ was the relative crystallinity at time t, K was the crystallization rate constant, and n was the Avrami exponent linked to the geometry of crystals. The linearization of Eq. (4) led to the following equation:

$$\ln[-\ln(1 - X_c)] = n\ln t + n\ln K \quad (7)$$

As shown in Fig. 4b, a series of straight lines were obtained from a plot of $\ln[-\ln(1-X_c)]$ versus lnt, indicating that the process obeyed the Avrami time dependence. From the linear fit of data in Fig. 4b, it was possible to determine the Avrami exponent n and the K constant, reported in Table 2. The values of n were consistent with other crystallization kinetic studies carried out on PET films (Lu and Hay, 2001). It should be underlined that this is the first study on the modeling of isothermal crystallization of PET microparticles. As expected, the values of Avrami rate constant values increased with the annealing temperature which favoured the molecular mobility. The highest K value was found at 160 °C suggesting that the crystallization process was occurring more rapidly. The value of 160 °C was then chosen as the annealing temperature for increasing the crystallization content of laboratory made microparticles.

Table 2
Avrami parameters of PET microplastics during isothermal crystallization at different temperatures.

Sample	n (-)	K (s^{-n})	R^2 (-)
PET-MP100	1.94	2.99×10^{-3}	0.996
PET-MP120	1.93	8.44×10^{-3}	0.999
PET-MP140	1.96	1.23×10^{-2}	0.998
PET-MP160	2.033	2.57×10^{-2}	0.997

Raman spectroscopy was employed to investigate the crystallinity of the samples. All spectra reported in Fig. 5a were normalized to the peak at 1291 cm^{-1}, corresponding to the ring and O–C stretching vibrations, as this band exhibited relatively constant intensity across samples (Perret et al., 2021). Three characteristic vibrational bands of PET were evident in the spectra. The peak at 1725 cm^{-1} was attributed to C=O stretching in the terephthalic acid units. The band at 1614 cm^{-1} was assigned to symmetric stretching of C—C/C=C bonds in the benzene ring. The band at 1118 cm^{-1} corresponded to the C—H rocking in the benzene ring and the C—O stretching in the ethylene glycol unit, while the band at 1096 cm^{-1} was associated with C(O)-O stretching of ester group and C—C stretching of ethylene glycol segment (Lionetto et al., 2022; Perret et al., 2021; Hafsia et al., 2016).

Numerous studies have shown that Raman spectroscopy is highly sensitive to the molecular conformations of PET. In particular, in the crystalline phase, the ethylene glycol units of PET molecule predominantly adopt a *trans* conformation, associated with a Raman peak near 1096 cm^{-1}. In contrast, both *trans* and gauche conformations coexist in the amorphous phase, corresponding to a peak around 1118 cm^{-1} (Perret et al., 2021; Hafsia et al., 2016; Ellis et al., 1995; Bouita et al., 2023). To gain deeper insight into the molecular conformations of PET, the spectral region between 1160 and 1040 cm^{-1} (Fig. 5b) has been investigated. The spectra show a vibrational band at 1096 cm^{-1} whose intensity and sharpness increase progressively with annealing temperature, particularly with the treatment at 160 °C. This behavior indicates enhanced molecular ordering or partial crystallization of the ethylene glycol-based segments. The spectral evolution from the amorphous to thermally treated states reflects a clear structural transition driven by thermal processing.

The integral intensities of the two vibrational bands at 1096 cm^{-1} and

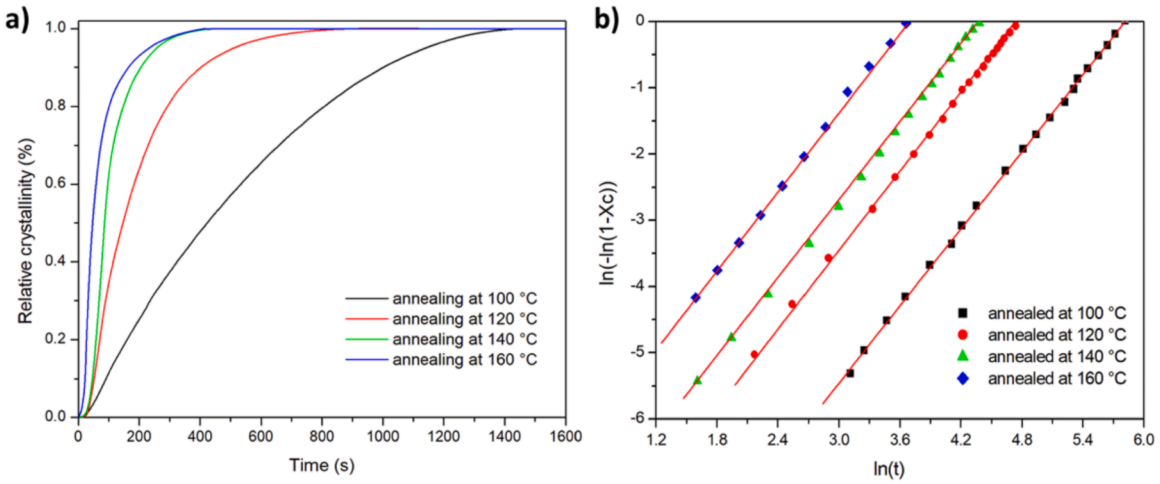

Fig. 4. a) Evolution of relative crystallinity as a function of time at different annealing temperatures; b) Avrami plot.

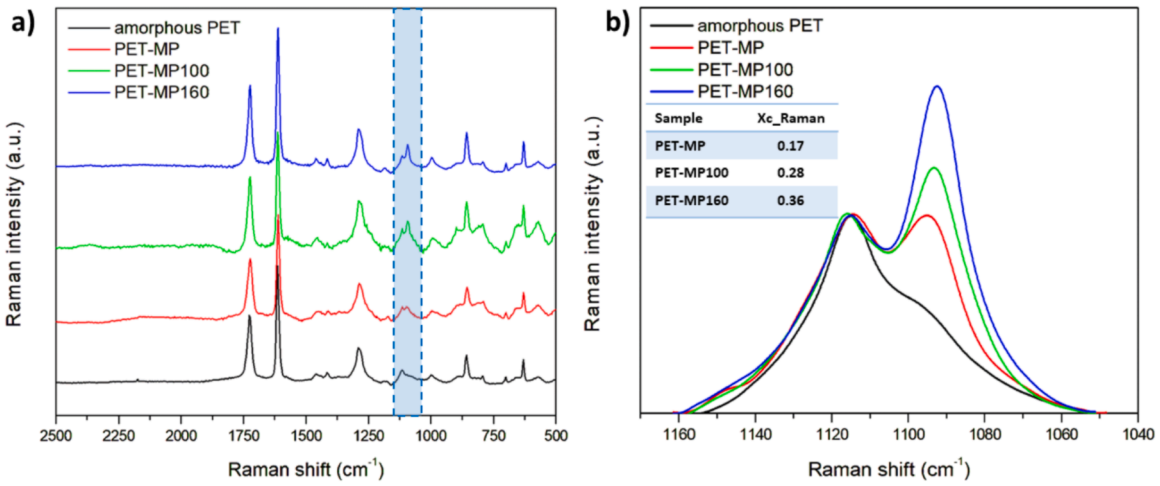

Fig. 5. a) Raman spectra of PET microparticles in different states: amorphous (black), mechanically processed (red), and thermally treated at 100 °C (green) and 160 °C (blue); b) magnified view of the 1160–1040 cm^{-1} region.

118 cm^{-1} can be used to assess a Raman relative crystallinity, $X_{c\text{-}Raman}$:

$$X_{c\_Raman} = \frac{I_{1096} - I_{1096a}}{I_{1118} + I_{1096}} \quad (8)$$

where I_{1096}, I_{1096a} and I_{1118} are the integral of the 1096 cm^{-1}, 1096 cm^{-1} in a 100 % amorphous state obtained in a quenched sample and 1118 cm^{-1} vibrational bands, respectively. The crystallization evolution with annealing temperature, as determined by the Raman ratio, followed a similar trend to that observed by DSC (Table 1), with values differing by no >15 %.

3.3. Autofluorescence characterization

To investigate the intrinsic fluorescence of the obtained PET NPs, a fluorescence characterization was performed by setting the excitation wavelengths and then recording the emission spectrum. In the 3D excitation-emission matrix (EEM) of label-free PET NPs reported in Fig. 6, each curve represented the fluorescence emission spectra at a specific excitation wavelength between 340 nm and 420 nm. The color gradient highlighted the intensity with the red area showing higher fluorescence intensity. As expected, emission spectra were strongly affected by the excitation wavelength. As reported in Fig. 6, label-free PET NPs exhibited wide-band fluorescence with a pronounced emission peak in the UV region (370–440 nm), followed by a distinct shoulder. The intrinsic fluorescence of PET was attributed to the phenylene rings in the backbone and their interaction with other phenylene rings or carbonyl groups (Lionetto et al., 2022).

The spectral properties of the true-to-life PET NPs make them suitable for fluorescence microscopy applications since they showed an excitation and emission peak compatible with the commercially available UV/violet light source and microscope's filters and detectors.

The visualization of PET NPs under confocal fluorescence microscopy is reported in Fig. 7, where a representative 3D reconstruction from PET NPs powder aggregates viewed by confocal fluorescence microscopy (with a 405 nm excitation laser line and a 425–475 nm emission filter) is reported. This laser line is commonly used in biological research to excite fluorophores with excitation peaks in the near-UV to violet range. The NPs aggregates were clearly visible with the UV/violet

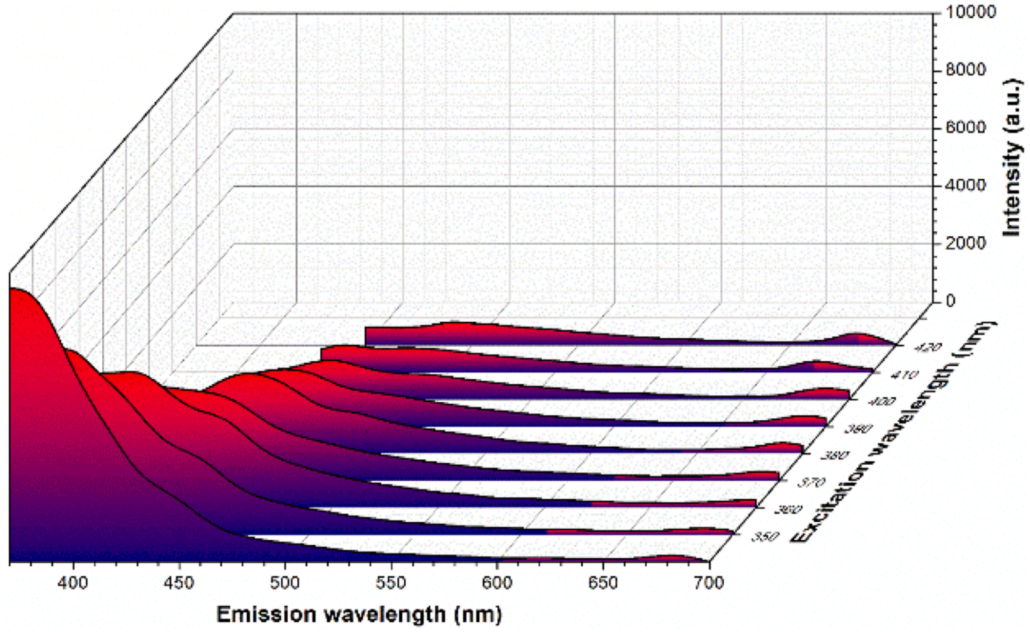

Fig. 6. Fluorescent emission spectra of label-free PET nanoplastics for different excitation wavelengths between 340 nm and 420 nm.

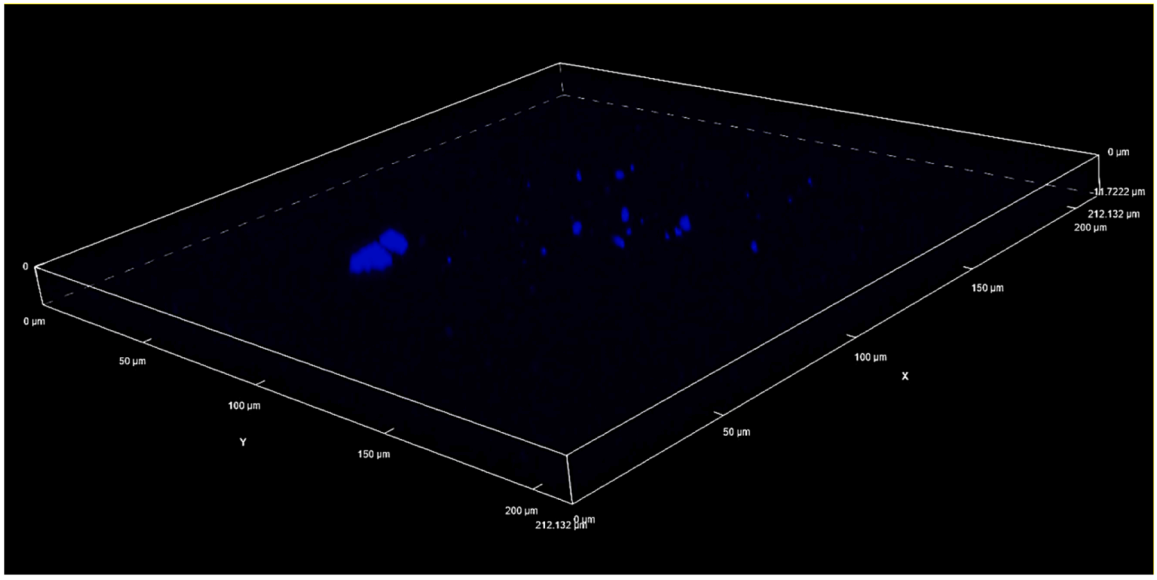

Fig. 7. 3D reconstruction of PET NP aggregates visualized under confocal microscopy by a 405 nm laser line of A1 NIKON confocal laser scanning unit coupled with a NIKON (Tokyo, Japan) Ti microscope. Objective used: Plan Apo 60 × 1.40 Oil.

laser line. Overall, the results confirm that PET NPs had intrinsic fluorescence properties that can be used for their detection and imaging in fluorescence microscopy and potentially in any fluorescence based technical approach or methodology without the addition of external dyes.

In this work, the potential of modulating the crystallinity of NPs to enhance the intensity of their fluorescence signal was explored by investigating two kinds of label-free PET NP samples with different apparent crystallinity, i.e. $X_c = 0.15$ after production and $X_c = 0.32$ after annealing. The same excitation wavelength (350 nm) was applied leading to fluorescence spectra with emission peaks centered at two different wavelengths, as shown in Fig. 8.

The observed blue shift and intensity enhancement with increasing crystallinity (Xc from 0.15 to 0.32) can be attributed to changes in the local packing of PET aromatic rings within the crystalline domains. In PET, the photophysically active units are the terephthalate aromatic rings, which generate weak monomeric fluorescence in the near-UV region. When the polymer undergoes mechanical processing (e.g. milling) or thermal treatment (annealing), its microstructure is modified in ways that strongly influence the excited-state dynamics. Mechanical fragmentation reduces crystallinity and introduces enhanced segmental

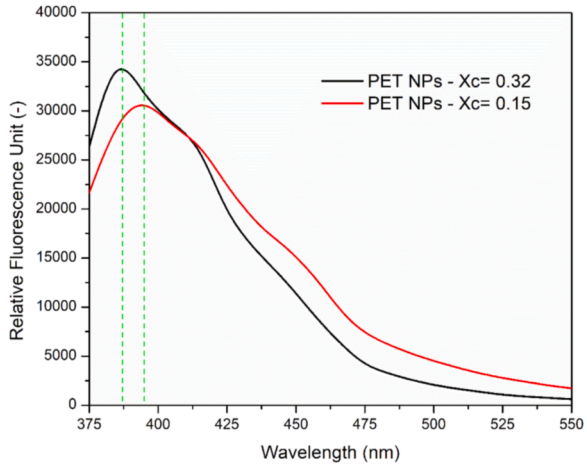

Fig. 8. Effect of crystallinity degree on the emission spectra of MPs excited at 350 nm.

mobility in the amorphous phase. These effects increase the probability of π–π interactions between neighboring aromatic rings, facilitating the formation of excimers. Thermal annealing promotes crystallization, reorganizes the surrounding amorphous regions and brings aromatic groups into more defined spatial arrangements, modifying their intermolecular interactions. This interpretation is consistent with the pioneering work of Itagaki (Itagaki et al., 1996), who demonstrated that PET fluorescence is highly sensitive to the degree of crystallinity. More recently, Zhao et al. (Zhao et al., 2023) reported that enhanced PET crystallization, induced by graphene quantum dots acting as nucleating agents, produces a marked increase in fluorescence intensity and a blue shift of the emission peak. They attributed this effect to the confinement of fluorescent centers within more ordered crystalline regions and the suppression of non-radiative decay. Together, these findings support our conclusion that the increase in fluorescence intensity and blue shift observed with higher PET crystallinity arise from molecular ordering and restricted chain dynamics within the crystalline domains.

Overall, the fluorescence characterization confirmed the capability to visualize label-free PET nanoparticles (obtained in the laboratory from post-consumer PET bottles) using spectrofluorimetric and microscopy techniques without the need for dye staining. This is possible due to the inherent fluorescence properties of PET. Such autofluorescence hold high potential for environmental applications both in detection of PET NPs in environmental samples or in studying their interaction with biological systems, since the autofluorescence could facilitate the identification and quantification of PET MNPs.

3.4. Ecotoxicological effects of label-free PET nanoplastics on Daphnia magna

To evaluate the potential ecotoxicological risk of PET NPs, we first assessed whether the freshwater zooplankton species *Daphnia magna* ingested the particles. We then investigated their effects on the viability of *Daphnia magna* under acute exposure conditions at different concentrations and temperatures. Finally, we evaluated the organisms' ability to recover after exposure and monitored for any delayed mortality.

3.4.1. Visualization of PET NPs in the body of Daphnia magna

Organisms were exposed to 5 mg/L of label-free PET NPs for 24 h and the distribution of label-free PET NPs in the body of *Daphnia magna* neonates was examined by fluorescence microscopy using a 360/460 nm

(blue) filter set. A prevalent accumulation in the gastrointestinal tract was evident in the neonates after 24 h, as shown in Fig. 9, while control organisms did not show any fluorescence. This result demonstrated that PET NPs were filtered and ingested by the organisms when they were exposed. It is known that *D. magna* feed by filtering microscopic particles from the water by generating water currents with their thoracic appendages. They draw food particles into their filtering apparatus and then ingest them (Turcihan et al., 2022). The filter mesh-sizes of *Daphnia magna* are in the size range of 0.24–0.64 μm (Geller and Müller, 1981). Therefore, based on the PET NPs distribution determined by DLS, it can be suggested that larger particles are efficiently captured trough filtration, while smaller particles may be ingested indirectly, either by attaching to larger particles or by being taken up during water intake.

3.4.2. PET NPs acute toxicity on Daphnia magna

The ecotoxicological effect of the exposure to PET NPs on *Daphnia magna* neonate survival was performed assessing immobilization of the animals after 48 h exposure. As reported in the Experimental section, neonates were exposed to different PET NPs concentrations in the range from 5 to 100 mg/L for 48 h at the temperatures of 21 °C and 25 °C. This broad range of concentrations was chosen to explore dose-dependent relationships according to literature data (Jemec et al., 2016). These concentrations are higher than the levels of NPs reported in natural waters which are usually below 1 μg/L. However, localized hotspots may occasionally reach higher levels (in the range of mg/L) due to pollution sources (Okoffo and Thomas, 2024; Shi et al., 2024). The concentrations used experimentally in this study were selected to assess acute toxicity which typically require higher concentrations than those found in nature to elicit clear, measurable effects within a short time frame, enabling dose-response analysis and hazard assessment, and simulating worst-case scenarios or spill/release events.

Moreover, our work was set up to evaluate the possible synergistic effects between temperature increase and exposure to NPs in the context of climate change. Climate change is causing global warming of surface waters, with freshwater ecosystems potentially experiencing even larger and more rapid fluctuations. A previous study by Na et al. (Na et al., 2023) on PET microplastics demonstrated a synergistic effect when *Daphnia magna* was exposed to both microplastics and increased temperature. However, to our knowledge, no information is currently available on the combined effects of PET NPs and temperature. A 4 °C increase, chosen in the present study, aligns with projections for near-future climate change scenarios often used in experimental studies to simulate future climate warming (Geerts et al., 2015; Bour et al., 2015).

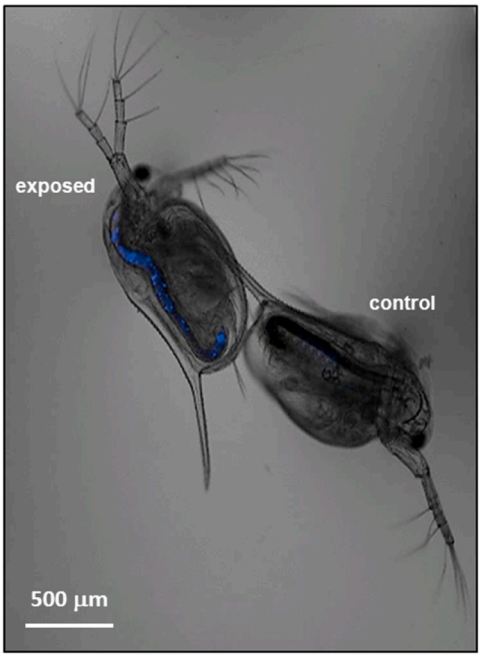

Fig. 9. Representative image of a *D. magna* neonate exposed for 24 h to label-free PET NPs and a control neonate. The two specimens were placed together in the same observation field. The displayed image is the result of merging the brightfield image with the fluorescence-acquired image (using a 360/460 nm filter set). Objective used: 4X.

Fig. 10a shows the mortality of *Daphnia magna* neonates exposed at 21 °C and 25 °C to label-free PET NPs in the concentration range from 5 mg/L to 100 mg/L for 48 h. No mortality was recorded at the temperature of 21 °C at any concentration tested while a weak dose-dependent decrease in the vitality of the organisms was observed at 25 °C, with a 15 % mortality at 100 mg/L. In all the tested experimental conditions, the mortality of control was 0, indicating the validity of the test according to EN ISO 6341:2012. These results indicate that PET NPs at the tested concentrations are not acutely lethal to *Daphnia magna* neonates at 21 °C, but higher temperatures (25 °C) increase their sensitivity, leading to measurable mortality. This suggests that increased temperature enhances the toxic effects of PET NPs on *Daphnia magna* neonates, possibly due to synergistic or additive stress. This highlights the importance of considering environmental factors like temperature when assessing the ecological risks of NPs.

3.4.3. Recovery assay

Following the 48 h exposure to label-free PET NPs, the organisms were exposed to clean water for another 48 h in order to assess their ability to recover after exposure. Previous studies on PET textile microfibers (Jemec et al., 2016) demonstrated that *Daphnia magna* exposed for 48 h were not able to recover in the subsequent 24 h post exposure, but data on possible recovery of *Daphnia* after exposure to PET NPs are lacking. In our experimental set up, after 48 h recovery, a dose-dependent increase in mortality was observed at both temperatures, and this effect was more pronounced at the exposure temperature of 25 °C (Fig. 10b). Controls did not show mortality in any experimental conditions. These results suggest that the PET NPs may have caused sublethal effects during the initial two-day exposure, leading to continued mortality even after the organisms were transferred to clean water.

As regards possible underlying mechanisms, NPs, including PET NPs, are known to generate intracellular oxidative stress in a wide range of cell types and organisms leading to downstream cellular effects (Giordano et al., 2025; Liu et al., 2020; Wang et al., 2024). Oxidative stress induction is a key multifaceted mechanism underlying NPs induced toxicity involving increased ROS (Bashirova et al., 2023), mitochondrial impairment (Bashirova et al., 2023; Zhang et al., 2022), and weakened antioxidant defenses, with downstream effects on gene expression and cell viability. Temperature increase can synergistically amplify ROS production (as shown in Lyu et al. (Lyu et al., 2021) for polystyrene MPs), potentially overwhelming the organism's antioxidant defense (Sanpradit et al., 2024). Such oxidative imbalance may cause cumulative cellular damage, which may become lethal only in the hours following exposure, coherently with the delayed mortality observed in our study.

These considerations highlight the potential for PET NPs to induce persistent damage even after direct exposure ends, raising concerns about their long-term effects that might extend beyond immediate exposure in a delayed and prolonged manner.

3.4.5. Comparison of the PET NPs ecotoxicological outcomes with literature data

Table 3 summarizes the few available data in literature on *Daphnia magna* mortality following exposure to PET MNPs under acute exposure conditions compared with results obtained in this study. The comparison highlights that the mortality rates observed in our study at 25 °C were

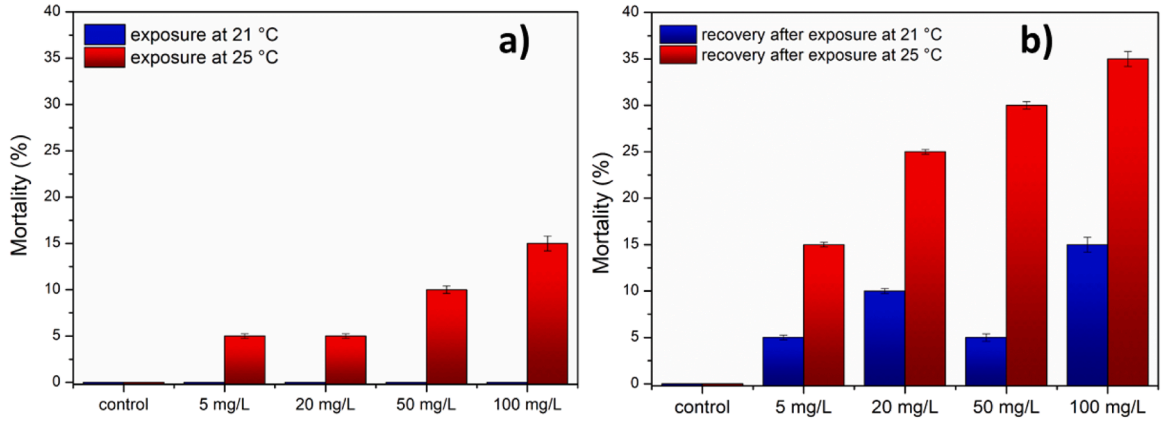

Fig. 10. Effect of PET NPs on the mortality of *Daphnia magna* neonates after 48 h exposure at two temperatures, 21 °C and 25 °C. Data are expressed as mean ± SD.

Table 3
Mortality data on *Daphnia Magna* exposed to micro-nanoplastics: comparison with previous literature.

Particle type	Average size (μm)	Concentration (mg/L)	Time of exposure (h)	Temperature (°C)	Mortality (%)	Ref.
PET fragments	33 ± 8	200	48	20 ± 1	20 at the highest concentration of 200 mg/L	(Han et al., 2021)
PET Fibres	360	100	48	20 ± 1	0	(Tourinho et al., 2022)
PET fibers	62–1400	12.5–100	48	21 ± 1	<10	(Jemec et al., 2016)
PET NPs	0.196	0.1–1000	48	20 ± 1	0	(Rajtar et al., 2025)
PET NPs	0.100	5–100 mg/L	48 h	21 ± 1	0	This study
		5–100 mg/L	48 h	26 ± 1	15–35	

generally higher than those reported in most studies conducted at lower temperatures, suggesting that temperature may enhance the toxicity of PET NPs. In contrast, at 21 °C, our results showed no mortality, which is in line with some of the previously reported findings for similar NP concentrations and exposure times. These differences underline the importance of environmental factors, such as temperature, in modulating the ecotoxicological effects of NPs on aquatic organisms. This interaction suggests that rising global temperatures could exacerbate the ecological impact of MNPs on aquatic organisms, emphasizing the need for environmental risk assessments that consider temperature variations. These findings highlight the importance of considering temperature as a significant factor in assessing the environmental risks of microplastics. Possible mechanisms underlying the observed effects of temperature could be represented by accelerated ingestion of NPs at increased temperature as demonstrated by Lyu et al. (Lyu et al., 2021) for polystyrene microplastics. This increased intake can lead to greater exposure to the toxic effects of the nanoplastics, thereby amplifying their negative impact on the organism's health and fitness. Moreover, elevated temperatures have been demonstrated by Lyu et al. (Lyu et al., 2021) to increase the expression of genes related to oxidative damage. This suggests that increased temperatures can enhance the oxidative stress caused by MNPs microplastics, further contributing to their toxicity.

4. Conclusions

Nanoplastics made from polyethylene terephthalate (PET) were successfully produced from post-consumer bottles using a top-down mechanical fragmentation process mimicking natural environmental degradation. These nanoparticles exhibited realistic physical properties, such as irregular shapes, with no alteration to the polymer's chemical structure. The nanoplastics were thoroughly characterized using multiple analytical techniques, including atomic force microscopy (AFM), laser diffraction, differential scanning calorimetry (DSC), Raman spectroscopy, confocal microscopy and fluorescence microscopy. The crystallinity of the nanoplastics was restored to mimic the ageing process of microplastics in the environment.

Label-free PET nanoplastics demonstrated intrinsic autofluorescence properties, making them suitable for fluorescence microscopy applications and potentially in any fluorescence based technical approach without the addition of external dyes. Higher crystallinity was found to be correlated with stronger fluorescence signals and a shift in emission peaks towards shorter wavelengths.

In this study, mechanically fragmented label-free PET nanoplastics were employed to investigate the role of crystallization kinetics in their autofluorescence behavior and to restore polymer crystallinity as a proxy for environmental aging. By avoiding UV and oxidative treatments, surface alterations were minimized, ensuring that the observed effects primarily reflected the intrinsic physical properties of the particles.In vivo exposure experiments with *Daphnia magna* validated the suitability of label-free PET nanoplastics for biological studies. The nanoplastics accumulated predominantly in the gastrointestinal tract of the organisms. Exposure to PET nanoplastics resulted in dose- and temperature-dependent mortality in *Daphnia magna*. Higher temperatures exacerbated the toxic effects, highlighting the potential for global warming to amplify the ecological impact of microplastics. PET nanoplastics induced sublethal effects during exposure, resulting in continued mortality even after the organisms were transferred to clean water. This raises concerns about their long-term ecological impact.

These findings highlight the importance of considering environmental factors, such as rising water temperatures due to climate change, in ecotoxicological risk assessments of NPs. Moreover, the use of label-free PET NPs with environmentally relevant properties represents a promising approach for future biological studies, supporting the need for standardized nanoplastic models in ecotoxicology.

Funding information

The authors declare that this research did not receive any specific grant from funding agencies in the public, commercial, or not-for-profit sectors.

CRediT authorship contribution statement

Francesca Lionetto: Writing – review & editing, Writing – original draft, Validation, Methodology, Investigation, Formal analysis, Data curation, Conceptualization. **Gregorio Polo:** Investigation. **Sonia Bagheri:** Investigation, Data curation. **Claudio Mele:** Writing – review & editing, Validation, Supervision, Methodology, Formal analysis, Data curation. **Carola Esposito Corcione:** Writing – review & editing, Validation, Supervision, Resources, Methodology, Formal analysis. **Maria Giulia Lionetto:** Writing – review & editing, Writing – original draft, Validation, Investigation, Formal analysis, Data curation, Conceptualization.

Declaration of competing interest

The authors declare that they have no known competing financial interests or personal relationships that could have appeared to influence the work reported in this paper.

Data availability

Data will be made available on request.

References

Yang, Z., Wang, M., Feng, Z., Wang, Z., Lv, M., Chang, J., Chen, L., Wang, C., 2023. Human microplastics exposure and potential health risks to target organs by different routes: a review. Curr. Pollut. Rep. 9, 468–485. https://doi.org/10.1007/s40726-023-00273-8.

Eo, S., Hong, S.H., Song, Y.K., Han, G.M., Shim, W.J., 2019. Spatiotemporal distribution and annual load of microplastics in the Nakdong River, South Korea. Water Res. 160, 228–237. https://doi.org/10.1016/j.watres.2019.05.053.

Cheng, H., Feng, Y., Duan, Z., Duan, X., Zhao, S., Wang, Y., Gong, Z., Wang, L., 2021. Toxicities of microplastic fibers and granules on the development of zebrafish embryos and their combined effects with cadmium. Chemosphere 269, 128677.

Besseling, E., Redondo-Hasselerharm, P., Foekema, E.M., Koelmans, A.A., 2019. Quantifying ecological risks of aquatic micro-and nanoplastic. Crit. Rev. Env. Sci. Technol. 49, 32–80.

Chae, Y., An, Y.-J., 2017. Effects of micro- and nanoplastics on aquatic ecosystems: current research trends and perspectives. Mar. Pollut. Bull. 124, 624–632. https://doi.org/10.1016/j.marpolbul.2017.01.070.

Serra, T., Vilaseca, F., Colomer, J., 2025. The chronic effects of polyethylene terephthalate and biodegradable polyhydroxybutyrate microplastics on Daphnia Magna. Environ. Res. 274, 121281.

Patrício Silva, A.L., Barceló, D., Rocha-Santos, T., 2024. Pharmaceuticals and micro (Nano)plastics in the environment: sorption and analytical challenges. Trends Environ. *Anal. Chem.* 44, e00243. https://doi.org/10.1016/j.teac.2024.e00243.

Gigault, J., Ter Halle, A., Baudrimont, M., Pascal, P.-Y., Gauffre, F., Phi, T.-L., El Hadri, H., Grassl, B., Reynaud, S., 2018. Current opinion: what is a nanoplastic? Environ. Pollut. 235, 1030–1034.

Polo, G., Lionetto, F., Giordano, M.E., Lionetto, M.G., 2024. Interaction of micro-and nanoplastics with enzymes: the case of carbonic anhydrase. Int. J. Mol. Sci. 25, 9716.

Giordano, M.E., Lionetto, F., Lionetto, M.G., 2025. Impact of polyethylene terephthalate nanoplastics (PET) on fibroblasts: a study on NIH-3T3 cells cells. Front. Physiol. 16, 1580682.

Hua, X., Wang, D., 2022. Cellular uptake, transport, and organelle response after exposure to microplastics and nanoplastics: current knowledge and perspectives for environmental and health risks. Rev. Environ. Contam. Toxicol. 260, 12. https://doi.org/10.1007/s44169-022-00013-x.

Bai, C.-L., Wang, D., Luan, Y.-L., Huang, S.-N., Liu, L.-Y., Guo, Y., 2024. A review on micro- and nanoplastics in humans: implication for their translocation of barriers and potential health effects. Chemosphere 361, 142424. https://doi.org/10.1016/j.chemosphere.2024.142424.

Nihart, A.J., Garcia, M.A., El Hayek, E., Liu, R., Olewine, M., Kingston, J.D., Castillo, E.F., Gullapalli, R.R., Howard, T., Bleske, B., et al., 2025. Bioaccumulation of microplastics in decedent Human brains. Nat. Med. 31, 1114–1119. https://doi.org/10.1038/s41591-024-03453-1.

Dong, X., Liu, X., Hou, Q., Wang, Z., 2023. From natural environment to animal tissues: a review of microplastics(Nanoplastics) translocation and hazards studies. Sci. Total Environ. 855, 158686. https://doi.org/10.1016/j.scitotenv.2022.158686.

Chang, X., Xue, Y., Li, J., Zou, L., Tang, M., 2020. Potential health impact of environmental micro-and nanoplastics pollution. J. Appl. Toxicol. 40, 4–15.

Nakano, H., Alfonso, M.B., Phinchan, N., Jandang, S., Manap, M.R.A., Chavanich, S., Viyakarn, V., Müller, M., Wong, C., Bacosa, H.P., 2025. Aquatic Microplastics research in the ASEAN Region: analysis of challenges and priorities. Mar. Pollut. Bull. 210, 117342.

Lettieri, R., Mudassir, M., Domenici, F., Salina, A., Venanzi, M., D'Ottavi, C., Di Bartolomeo, E., Gatto, E., 2025. Control of nanoparticle size of intrinsically fluorescent PET (Polyethylene Terephthalate) particles produced through nanoprecipitation. Molecules 30, 282.

Ramsperger, A.F.R.M., Jasinski, J., Völkl, M., Witzmann, T., Meinhart, M., Jérôme, V., Kretschmer, W.P., Freitag, R., Senker, J., Fery, A., et al., 2022. Supposedly identical microplastic particles substantially differ in their material properties influencing particle-cell interactions and cellular responses. J. Hazard. Mater. 425, 127961. https://doi.org/10.1016/j.jhazmat.2021.127961.

World Health Organization Dietary and inhalation exposure to nano-and microplastic particles and potential implications for Human health. In *Dietary and Inhalation Exposure to Nano-And Microplastic Particles and Potential Implications for Human Health*; 2022.

Santizo, K.Y., Mangold, H.S., Mirzaei, Z., Park, H., Kolan, R.R., Sarau, G., Kolle, S., Hansen, T., Christiansen, S., Wohlleben, W., 2025. Microplastic materials for inhalation studies: preparation by solvent precipitation and comprehensive characterization. Small, 2405555.

Ducoli, S., Kalčíková, G., Velimirovic, M., Depero, L.E., Federici, S., 2025. Production, characterization, and toxicology of environmentally relevant nanoplastics: a review. Environ. Chem. Lett. 1–27.

Crosset-Perrotin, G., Moraz, A., Portela, R., Alcolea-Rodriguez, V., Burrueco-Subirà, D., Smith, C., Bañares, M.A., Foroutan, H., Fairbrother, D.H., 2025. Production, labeling, and applications of micro-and nanoplastic reference and test materials. Environ. Sci. Nano 12, 2911–2964.

Lionetto, F., Lionetto, M.G., Mele, C., Corcione, C.E., Bagheri, S., Udayan, G., Maffezzoli, A., 2022. Autofluorescence of model polyethylene terephthalate nanoplastics for cell interaction studies. Nanomaterials 12, 1560.

Ducoli, S., Federici, S., Cocca, M., Gentile, G., Zendrini, A., Bergese, P., Depero, L.E., 2024. Characterization of polyethylene terephthalate (PET) and polyamide (PA) true-to-life nanoplastics and their biological interactions. Environ. Pollut. 343, 123150. https://doi.org/10.1016/j.envpol.2023.123150.

Rajabimashhadi, Z., Gallo, N., Russo, F., Ghiyami, S., Mele, C., Giordano, M.E., Lionetto, M.G., Salvatore, L., Lionetto, F., 2024. Production and physico-chemical characterization of nano-sized collagen from equine tendon. Int. J. Biol. Macromol. 277, 134220.

Aljoumaa, K., Abboudi, M., 2015. Physical ageing of polyethylene terephthalate under natural sunlight: correlation study between crystallinity and mechanical properties. Appl. Phys. A 122, 6. https://doi.org/10.1007/s00339-015-9518-0.

Jovanović, A., Bugarčić, M., Simić, M., Pejić, J., Dimitrijević, J., 2025. The global market of PET production: from origins to recycling. Met. Mater. Data 2, 113–118.

Greco, A., Lionetto, F., Maffezzoli, A., 2015. Processing and characterization of amorphous polyethylene terephthalate fibers for the alignment of carbon nanofillers in thermosetting resins. Polym. Compos. 36, 1096–1103.

Alaraby, M., Abass, D., Velázquez, A., Hernández, A., Marcos, R., 2025. Occurrence, analysis, and toxicity of polyethylene terephthalate microplastics: a review. Environ. Chem. Lett. 1–35.

Briga-Sá, A., Ferreira, L., Paulo, B., Bentes, I., Teixeira, C.A., 2023. Energy and Environmental performance assessment of reused PET bottles panels for building thermal insulation solutions. Energy Build. 298, 113529.

Kumar, V., Sharma, N., Umesh, M., Sharma, R., Sharma, M., Sharma, D., Sharma, M., Sondhi, S., Thomas, J., Kumar, D., et al., 2024. Commercialization potential of PET (Polyethylene Terephthalate) recycled nanomaterials: a review on validation parameters. Chemosphere 352, 141453. https://doi.org/10.1016/j.chemosphere.2024.141453.

Vetter, C.B., Hildebrandt, L., Zimmermann, T., Schmidt, C.E., El Gareb, F., Mitrano, D.M., Pröfrock, D., Thomas, H., 2025. Analysis of microplastics in the fjords of Tunu (East Greenland). Mar. Pollut. Bull. 218, 118192. https://doi.org/10.1016/j.marpolbul.2025.118192.

Rajtar, N., Starek, M., Vincenti, L., Dąbrowska, M., Romek, M., Rinaldi, R., Lionetto, F., Kepczynski, M., 2025. Effect of PET micro/nanoplastics on model freshwater zooplankton. Polymers 17, 1256.

Freilinger, J., Kappacher, C., Huter, K., Hofer, T.S., Back, J.O., Huck, C.W., Bakry, R., 2025. Interactions between perfluorinated alkyl substances (PFAS) and microplastics (MPs): findings from an extensive investigation. J. Hazard. Mater. Adv. 18, 100740. https://doi.org/10.1016/j.hazadv.2025.100740.

Lionetto, F., Esposito Corcione, C., Messa, F., Perrone, S., Salomone, A., Maffezzoli, A., 2023. The sorption of amoxicillin on engineered polyethylene terephthalate microplastics. J. Polym. Environ. 31, 1383–1397.

Liu, S., Liu, X., Guo, J., Yang, R., Wang, H., Sun, Y., Chen, B., Dong, R., 2023. The association between microplastics and microbiota in placentas and meconium: the first evidence in humans. Environ. Sci. Technol. 57, 17774–17785. https://doi.org/10.1021/acs.est.2c04706.

Cho, E., Ji, S., Moon, J., Koh, H.R., 2025. Fluorescence imaging of microplastics and nanoplastics in biological samples. Mol. Cell. Toxicol. 1–8.

Ebert, D., 2022. Daphnia as a versatile model system in ecology and evolution. Evodevo 13, 16. https://doi.org/10.1186/s13227-022-00199-0.

Le, Q.-A.V., Sekhon, S.S., Lee, L., Ko, J.H., Min, J., 2016. Daphnia in water quality biomonitoring - "omic" approaches. Toxicol. Environ. Health Sci. 8, 1–6. https://doi.org/10.1007/s13530-016-0255-3.

Rosner, A., Ballarin, L., Barnay-Verdier, S., Borisenko, I., Drago, L., Drobne, D., Concetta Eliso, M., Harbuzov, Z., Grimaldi, A., Guy-Haim, T., 2024. A broad-taxa approach as an important concept in ecotoxicological studies and pollution monitoring. Biol. Rev. 99, 131–176.

Lionetto, F., Corcione, C.E., Rizzo, A., Maffezzoli, A., 2021. Production and characterization of polyethylene terephthalate nanoparticles. Polymers 13, 3745.

Chang, X., Hallais, S., Danas, K., Roux, S., 2023. PeakForce AFM analysis enhanced with model reduction techniques. Sensors 23, 4730.

Rodríguez Chialanza, M., Sierra, I., Pérez Parada, A., Fornaro, L., 2018. Identification and quantitation of semi-crystalline microplastics using image analysis and differential scanning calorimetry. Environ. Sci. Pollut. Res. 25, 16767–16775.
Šudomová, L., Doležalová Weissmannová, H., Steinmetz, Z., Řezáčová, V., Kučerík, J., 2023. A differential scanning calorimetry (DSC) approach for assessing the quality of polyethylene terephthalate (PET) waste for physical recycling: a proof-of-concept study. J. Therm. Anal. Calorim. 148, 10843–10855.
EN ISO 6341: 2012 Water quality determination of the inhibition of the mobility of Daphnia Magna Strauss (Cladocera, Crustacean).
Development, O. for E.C, 2004. Test No. 202: Daphnia Sp. Acute Immobilisation Test. OECD publishing. ISBN 9264069941.
David, R.M., Dakic, V., Williams, T.D., Winter, M.J., Chipman, J.K., 2011. Transcriptional responses in neonate and adult daphnia magna in relation to relative susceptibility to genotoxicants. Aquat. Toxicol. 104, 192–204. https://doi.org/10.1016/j.aquatox.2011.04.016.
ASTM, E., 1980. 729-80; Standard practice for conducting acute toxicity tests with fishes, macroinvertebrates and amphibians. Am. Stand. Test. Mater. Corvallis, Oregon, USA.
Bergman Filho, T.U., Soares, A.M.V.M., Loureiro, S., 2011. Energy budget in Daphnia Magna exposed to natural stressors. Environ. Sci. Pollut. Res. 18, 655–662. https://doi.org/10.1007/s11356-010-0413-0.
Im, H., Na, J., Jung, J., 2020. The effect of food availability on thermal stress in Daphnia Magna: trade-offs among oxidative stress, somatic growth, and reproduction. Aquat. Ecol. 54, 1201–1210. https://doi.org/10.1007/s10452-020-09804-7.
De Pascalis, F., Lionetto, F., Maffezzoli, A., Nacucchi, M., 2023. A general approach to calculate the stiffness tensor of short-Fiber composites using the fabric tensor determined by X-ray computed tomography. Polym. Compos. 44, 917–931. https://doi.org/10.1002/pc.27143.
Font, J., Muntasell, J., Cesari, E., 1999. Effect of milling on the thermal behaviour of poly (Ethylene Terephthalate). Thermochim. Acta 333, 169–172.
Zaker, A., Auclair, K., 2024. Impact of ball milling on the microstructure of polyethylene terephthalate. ChemSusChem, e202401506.
Bai, C., Spontak, R.J., Koch, C.C., Saw, C.K., Balik, C.M, 2000. Structural changes in poly (Ethylene Terephthalate) induced by mechanical milling. Polymer 41, 7147–7157.
Viora, L., Combeau, M., Pucci, M.F., Perrin, D., Liotier, P.-J., Bouvard, J.-L., Combeaud, C., 2023. A comparative study on crystallisation for Virgin and recycled polyethylene terephthalate (PET): multiscale effects on physico-mechanical properties. Polymers 15, 4613.
Androsch, R., Wunderlich, B., 2005. The link between rigid amorphous fraction and crystal perfection in cold-crystallized poly (Ethylene Terephthalate). Polymer (Guildf) 46, 12556–12566.
Lu, H., Diaz, D.J., Czarnecki, N.J., Zhu, C., Kim, W., Shroff, R., Acosta, D.J., Alexander, B. R., Cole, H.O., Zhang, Y., 2022. Machine learning-aided engineering of hydrolases for PET depolymerization. Nature 604, 662–667.
Thomsen, T.B., Almdal, K., Meyer, A.S., 2023. Significance of poly (Ethylene Terephthalate)(PET) substrate crystallinity on enzymatic degradation. N. Biotechnol.
Guo, X., Wang, J., 2019. The chemical behaviors of microplastics in marine environment: a review. Mar. Pollut. Bull. 142, 1–14. https://doi.org/10.1016/j.marpolbul.2019.03.019.
Bartolotta, A., Di Marco, G., Farsaci, F., Lanza, M., Pieruccini, M., 2003. DSC and DMTA study of annealed cold-drawn PET: a three phase model interpretation. Polymer (Guildf) 44, 5771–5777. https://doi.org/10.1016/S0032-3861(03)00589-5.
Badia, J.D., Strömberg, E., Karlsson, S., Ribes-Greus, A., 2012. The role of crystalline, mobile amorphous and rigid amorphous fractions in the performance of recycled poly (Ethylene Terephthalate)(PET). Polym. Degrad. Stab. 97, 98–107.
Corcione, C.E., Maffezzoli, A., 2009. Glass transition in thermosetting clay-nanocomposite polyurethanes. Thermochim. Acta 485, 43–48.
Avrami, M., 1939. Kinetics of phase change. I General theory. J. Chem. Phys. 7, 1103–1112.
Lu, X.F., Hay, J.N., 2001. Isothermal crystallization kinetics and melting behaviour of poly (Ethylene Terephthalate). Polymer (Guildf) 42, 9423–9431.
Perret, E., Braun, O., Sharma, K., Tritsch, S., Muff, R., Hufenus, R., 2021. High-resolution 2D raman mapping of mono-and bicomponent filament cross-sections. Polymer (Guildf) 229, 124011.
Hafsia, K.Ben, Ponçot, M., Chapron, D., Royaud, I., Dahoun, A., Bourson, P., 2016. A novel approach to study the isothermal and non-isothermal crystallization kinetics of poly (Ethylene Terephthalate) by raman spectroscopy. J. Polym. Res. 23, 1–14.
Ellis, G., Roman, F., Marco, C., Gomez, M.A., Fatou, J.G., 1995. FT raman study of orientation and crystallization processes in poly (Ethylene Terephthalate). Spectrochim. Acta Part A Mol. Biomol. Spectrosc. 51, 2139–2145.
Bouita, M., Tinnes, J., Bourson, P., Malfois, M., Ponçot, M., 2023. A new raman spectroscopy-based method for monitoring the crystallinity ratio of polyethylene terephthalate. J. Raman Spectrosc. 54, 225–232.
Itagaki, H., Inagaki, Y., Kobayashi, N., 1996. Microenvironments in poly (Ethylene Terephthalate) film revealed by means of fluorescence measurements. Polymer (Guildf) 37, 3553–3558.
Zhao, L., Yin, Y., Xiao, W., Li, H., Feng, H., Wang, D., Qu, C., 2023. Rapid crystallization and fluorescence of Poly (Ethylene Terephthalate) using graphene quantum dots as nucleating agents. Polymers 15, 3506.
Turcihan, G., Isinibilir, M., Zeybek, Y.G., Eryalçın, K.M., 2022. Effect of different feeds on reproduction performance, nutritional components and fatty acid composition of Cladocer water flea (Daphnia Magna). Aquac. Res. 53, 2420–2430.
Geller, W., Müller, H., 1981. The filtration apparatus of Cladocera: filter mesh-sizes and their implications on food selectivity. Oecologia 49, 316–321. https://doi.org/10.1007/BF00347591/METRICS.
Jemec, A., Horvat, P., Kunej, U., Bele, M., Kržan, A., 2016. Uptake and effects of microplastic textile fibers on freshwater crustacean Daphnia Magna. Environ. Pollut. 219, 201–209. https://doi.org/10.1016/j.envpol.2016.10.037.
Okoffo, E.D., Thomas, K., 2024. V quantitative analysis of nanoplastics in environmental and potable waters by pyrolysis-gas chromatography–Mass spectrometry. J. Hazard. Mater. 464, 133013. https://doi.org/10.1016/j.jhazmat.2023.133013.
Shi, C., Liu, Z., Yu, B., Zhang, Y., Yang, H., Han, Y., Wang, B., Liu, Z., Zhang, H., 2024. Emergence of nanoplastics in the aquatic environment and possible impacts on aquatic organisms. Sci. Total Environ. 906, 167404. https://doi.org/10.1016/j.scitotenv.2023.167404.
Na, J., Song, J., Jung, J., 2023. Elevated temperature enhanced lethal and sublethal acute toxicity of polyethylene microplastic fragments in Daphnia Magna. Environ. Toxicol. Pharmacol. 102, 104212.
Geerts, A.N., Vanoverbeke, J., Vanschoenwinkel, B., Van Doorslaer, W., Feuchtmayr, H., Atkinson, D., Moss, B., Davidson, T.A., Sayer, C.D., De Meester, L., 2015. Rapid evolution of thermal tolerance in the water flea daphnia. Nat. Clim. Chang. 5, 665–668. https://doi.org/10.1038/nclimate2628.
Bour, A., Mouchet, F., Silvestre, J., Gauthier, L., Pinelli, E., 2015. Environmentally relevant approaches to assess nanoparticles ecotoxicity: a review. J. Hazard. Mater. 283, 764–777. https://doi.org/10.1016/j.jhazmat.2014.10.021.
Liu, Z., Huang, Y., Jiao, Y., Chen, Q., Wu, D., Yu, P., Li, Y., Cai, M., Zhao, Y., 2020. Polystyrene nanoplastic induces ROS production and affects the MAPK-HIF-1/NFkB-mediated antioxidant system in Daphnia Pulex. Aquat. Toxicol. 220, 105420. https://doi.org/10.1016/j.aquatox.2020.105420.
Wang, Y., Huang, Y., Fu, L., Wang, X., Chen, L., 2024. Evaluation of nanoplastics-induced redox imbalance in cells, larval zebrafish, and daphnia magna with a superoxide anion radical fluorescent probe. Chemosphere 356, 141829. https://doi.org/10.1016/j.chemosphere.2024.141829.
Bashirova, N., Poppitz, D., Klüver, N., Scholz, S., Matysik, J., Alia, A., 2023. A mechanistic understanding of the effects of polyethylene terephthalate nanoplastics in the zebrafish (Danio Rerio) embryo. Sci. Rep. 13, 1–14. https://doi.org/10.1038/s41598-023-28712-y.
Zhang, H., Zhang, S., Duan, Z., Wang, L., 2022. Pulmonary toxicology assessment of polyethylene terephthalate nanoplastic particles in vitro. Environ. Int. 162, 107177. https://doi.org/10.1016/j.envint.2022.107177.
Lyu, K., Cao, C., Li, D., Akbar, S., Yang, Z., 2021. The thermal regime modifies the response of aquatic keystone species daphnia to microplastics: evidence from population fitness, accumulation, histopathological analysis and candidate gene expression. Sci. Total Environ. 783, 147154. https://doi.org/10.1016/j.scitotenv.2021.147154.
Sanpradit, P., Byeon, E., Lee, J.-S., Jeong, H., Kim, H.S., Peerakietkhajorn, S., Lee, J.-S., 2024. Combined effects of nanoplastics and elevated temperature in the freshwater water flea Daphnia Magna. J. Hazard. Mater. 465, 133325. https://doi.org/10.1016/j.jhazmat.2023.133325.
Han, B., Geonu, P., Yoo, S., Kim, C., Jung, J., 2021. Effect of chronic toxicity by waste microplastics (PET) on Daphnia Magna. Ecol. Resilient Infrastruct. 8, 281–289.
Tourinho, P.S., Silva, A.R.R., Santos, C.S.A., Prodana, M., Ferreira, V., Habibullah, G., Kočí, V., van Gestel, C.A.M., Loureiro, S., 2022. Microplastic fibers increase sublethal effects of AgNP and AgNO3 in Daphnia Magna by changing cellular energy allocation. Environ. Toxicol. Chem. 41, 896–904.